Optimization of Metallic Powder Filaments for Additive Manufacturing Extrusion (MEX)

Fábio Silva Cerejo (fcerejo@ipn.pt)
Instituto Pedro Nunes, Pedro Nunes street, 3030-199 Coimbra, Portugal https://orcid.org/0000-0002-1567-2382

Daniel Gatões
University of Coimbra, CEMMPRE, Department of Mechanical Engineering, Luís Reis Santos street, 3030-788 Coimbra, Portugal

Teresa Vieira
University of Coimbra, CEMMPRE, Department of Mechanical Engineering, Luís Reis Santos street, 3030-788 Coimbra, Portugal

Research Article

Keywords: MEX, Filament, Additive Manufacturing, Mixing Torque, Austenitic Stainless Steel (316L)

Posted Date: February 9th, 2021

DOI: https://doi.org/10.21203/rs.3.rs-168766/v1

Abstract

Additive manufacturing (AM) of metallic powder particles has been establishing itself as sustainable, whatever the technology selected. Material Extrusion (MEX) integrates the ongoing effort to improve AM sustainability, in which low-cost equipment is associated with a decrease of powder waste during manufacturing. MEX has been gaining increasing interest for building 3D functional/structural metallic parts because it incorporates the consolidated knowledge from powder injection moulding/extrusion feedstocks into the AM scope—filament extrusion layer-by-layer. Moreover, MEX as an indirect process can overcome some of the technical limitations of direct AM processes (laser/electron-beam-based) regarding energy-matter interactions. The present study reveals an optimal methodology to produce MEX filament feedstocks (metallic powder, binder and additives), having in mind to attain the highest metallic powder content. Nevertheless, the main challenges are also to achieve high extrudability and a suitable ratio between stiffness and flexibility. The metallic powder volume content (vol.%) in the feedstocks was evaluated by the critical powder volume concentration (CPVC). Subsequently, the rheology of the feedstocks was established by means of the mixing torque value, which is related to the filament extrudability performance.

Introduction

Additive manufacturing (AM) of powder metals and metal alloys is an unavoidable area for Industry 4.0 owing to its potential to address some of the most significant industrial challenges in the twenty-first century concerning parts/system/devices processing [1]. The rising trend to select AM processes is based on new design approaches; the ability to create near net shape 3D objects; cloud access to manufacturing; shorter time-to-market; product customisation; and circular economy [2]. Among other factors, the possibility of merging cost savings and new part properties and features that are impossible to obtain using traditional manufacturing technologies is the largest benefit of AM. This manufacturing paradigm, concerning powder metal AM, has attracted significant interest over the past few years, where AM direct methods (e.g. SLM, EBM…) established themselves as technologies for functional/structural metallic parts, with several components approved by ISO and ASTM standards in industries such as aerospace and automotive [3]. However, these processes have several drawbacks, the high-power source that can promote micro and macroscopic defects in metallic parts due to the multiple thermal treatments of the deposited layers; material range, due to the energy-matter interaction that limits the powder characteristics, like reflectivity and conductivity; significant powder wastes during manufacturing and handling hazard. Besides, the high cost of direct AM equipment is one of the major obstacles [4–11].

Material extrusion (MEX) and binder jetting (BJ) [12] are already well-established technologies with market acceptance for the AM. Based on this successful background, MEX and BJ have been investigated with the aim to produce metallic and ceramic functional/structural components through shaping, debinding and sintering (SDS). In this indirect AM processes, unlike direct methods, the material processability is independent of the power source, which makes the production of functionally-graded materials feasible [13]. Regarding shaping, BJ and MEX differ from each other. In BJ, the binder droplets

are selectively deposited to interact with powder particles, which presents new challenges not associated with MEX, such as powder/binder wettability; binder vertical migration, since layer height affects the penetration depth of the binder, through time and capillary force; and binder saturation that must be fine-tuned, as well as droplet size and dispensing frequency. However, the metallic powder is fed independently of the binder, which makes the rheological properties not as hard to control as it happens with MEX, which is beneficial to achieve the highest vol.% of metallic powder and less binder content in the shaped 3D object [13, 14]. Even though both technologies differ in what concerns the powder-binder processability, they also face the same challenges, such as optimizing debinding heating profiles to degrade the polymer is time-consuming; possible undesired reactions from residual polymer ash that could affect the final properties; and porosity, since both technologies do not have high pressures that promote the highest final part densification [13, 15].

The present study is focused on the MEX technology, which was initially referred to as the fused deposition of metals (FDMet), and then as Fused Filament Fabrication (FFF) or as Metallic Fused Filament Fabrication (MF^3) [16]. MEX is based on the fused deposition modelling (FDM^{TM}) technology commercialised by Stratasys Inc. for polymers and waxes, where the filament is composed of a mixture of a high volume content (vol.%) of metallic powders with organic constituents [17]. MEX is suitable for manufacturing geometrical complex metal parts in conjunction with post-shaping steps, such as debinding and sintering [18].

The processing by MEX technology consists of 5 stages (Fig. 1), as follows: Stages 1 and 2 –powder material extrusion feedstocks fabrication, where is fundamental to attain the highest content (%vol) and homogeneity of metallic powders within a selected master binder and other additives to guarantee an appropriate viscosity and an excellent balance between flexibility and stiffness; Stage 3 - concerns feedstock extrusion; Stage 4 - 3D part/device building (green) from filament deposited layer-by-layer; Stage 5 - binder removal (debinding) and subsequent consolidation of metallic powder particles (sintering).

High quality structural/functional parts/systems/devices through an SDS process, must include efforts to achieve the highest content (vol.%) of the metallic powder particles possible in the feedstock within the steady-state regime, but always taking into account the final mixing torque value. This becomes a significant challenge in MEX because the mixture must be manufactured in a filament form. Based on these assumptions, there are a few available studies in the bibliography. Agarwala et al. obtained stiff and straight filaments from feedstocks with 60 vol.% 17-4PH grade stainless steel (SS) [19]. Kukla and Gutierrez et al. [20, 21] used 55 vol.% SS 316L and 17-4PH, Godec et al. [10] also selected 55 vol.% SS 316L, as well as Burkhardt et al. [22]. Anderson et al. [23] produced SS 316L grade filaments with 55 vol.%, Kurose et al. [24] used SS 316L grade filaments with 60 vol.%. Gloeckle et al. [25] performed an extensive study on the printability of Ti-6Al-4V filaments with up to 60 vol.% of inorganic material and Singh et al. [16] used the same Ti-6Al-4V with 59 vol.%. BASF SE® has a commercially available SS 316L filament with a metallic powder content lower than 60 vol.% [26].

The mechanical performance of MEX metallic filaments has been a major limitation for increasing the ratio between inorganic and organic constituents since high powder concentration can lead to poor extrudability, where the filament becomes too brittle to be handled. A balance between stiffness and flexibility must be guaranteed to promote filament printability [16, 20].

The focus of the present study is to develop filaments with the highest metallic powder volume content (>50 vol.%) that link the primary MEX filament requirements to a suitable viscosity and mechanical behaviour. The selection of the highest content of metallic powder was evaluated by critical powder volume concentration (CPVC) methodology [27–29]. This procedure aims to promote the highest part green density, which is essential for maintaining the part shape integrity after debinding and sintering.

The present study aims to contribute, whatever the powder selected, to high-quality filaments for MEX technology, that is in conjunction with binder jetting technology, the future of AM of functional/structural 3D metallic objects.

Materials And Methods

2.1 Characterisation techniques

The characterisations of the powders, feedstocks and filaments were performed through the following techniques: laser diffraction to measure the particle size (Malvern Mastersizer 2000); helium pycnometry to measure the density (Micromeritics AccuPyc 1330); scanning electron microscopy (SEM) to analyse the morphology and shape factor (FEI Quanta 400FEG) x-ray diffraction (XRD), to identify the phases (Phillip's X'Pert, cobalt radiation $\lambda_{k\alpha1}$= 0.1789 nm and $\lambda_{k\alpha2}$= 0.1793 nm, Bragg-Brentano geometry); and TGA to analyse the weight variation kinetics (TGA Q500 V20.13). The filament was micro-CT (X-ray micro computed tomography) scanned using a Bruker SkyScan 1275. An acceleration voltage of 80 kV and a beam current of 125 µA was set while using a 1mm Aluminium filter and step-and-shoot mode. Pixel size was set to 6 µm and random mode was used. 1056 projection images were acquired at 0.2˚ angular step with 5 frames average per step using an exposure time of 46 ms. The micro-CT images were reconstructed with the dedicated manufacturer software.

Three-point flexural test of the filaments was performed using SHIMADZU-EZ-LX equipment with a load capacity of 500 N. The load was applied to the specimen at a rate of 0.5 mm/min.

Hardness measurements were performed with a Shimadzu HMV microhardness tester. For each measurement, a load of 9.8 N was applied for 15 seconds by a Vickers indenter.

2.2 Metallic powder, binder and additives

The set material for this study was austenitic stainless steel 316L (SS 316L) since it is one of the most studied materials in AM. This material can be a good standard for the methodology to be established by the present work and extrapolated to other metallic alloys [30].

The characteristics of the selected powders were studied using the 4S's methodology (Size and Size distribution, Shape and Structure). The particle size is d_{50} = 9.43 µm. Fig. 2 shows the particle size distribution (a), particle shape factor (b). Shape factor was close to 1 for the nitrogen atomised SS 316L powders (Osprey Sandvik®).

Table 1 summarises the powder characteristics.

Table 1. SS 316L powder characteristics

d_{10} [µm]	d_{50} [µm]	d_{90} [µm]	SSA* [kg/m^2]	ρ [kg/m^3] **
4.63	9.43	16.60	786	7896 ± 30.2

* Specific Surface Area

**Density

The X-ray diffractogram (Fig. 3) of the SS 316L powder exhibited a biphasic character, where the major phase was austenite (ICDD 33-0397). However, other peaks with low I/I_0 were present, which can be indexed as (100), (200) that are typical of ferrite/martensite (ICDD 87-0722). The cooling stress could contribute to the evolution of the austenite phase into martensite. Nevertheless, nitrogen atomising results in lower stress in the particles than those from water atomising, where martensite is more prevalent for a similar powder [31].

In the present study, the organic constituents of the feedstocks were divided into two primary groups: master binder and additives; the last one includes the backbone and surfactant/plasticiser. The selected master binder (M1) was a commercial-grade (Atect®) that is a mixture of polyolefin waxes and > 60 wt. %) of polyoxymethylene (POM) The thermoplastic elastomer (TPE), as well as an ultra-low density polyethylene (ULD-PE), was used for the backbone, a surfactant (stearic acid (S□)) and an external plasticiser (P X). Table 2 summarises the densities of the master binder and additives.

Table 2. *Densities of the binder and additives measured with a helium pycnometer (Micromeritics AccuPyc 1330)*

	M1	TPE	ULD-PE	S□	P X
Density [kg/m^3]	970 ± 1	1028 ± 12.2	9144 ± 1.5	983 ± 1	965 ± 0.6

$S^{\square}$ Surfactant

P^{X} Plasticiser

2.3 Filaments processing from green to sintered

The vol.% of each organic component in the feedstock was tailored to achieve the proper filament properties for MEX (rheology and flexibility/stiffness balance). The CPVC and feedstock optimisation was performed with a torque rheometer (Plastograph® Brabender GmbH & Co. KG) that evaluates the torque variation as a function of the powder composition. A temperature of 180 °C was selected, taking into account previous work with the same master binder [31]. The rotation of the blades was set at 30 rpm. For the CPVC evaluation an increment of 1 vol.% powder content was made approximately every 10 minutes, or after reaching a steady state. The backbone percentage was not higher than 30% of the total organic portion. Table 3 summarises the different feedstock compositions (F01–F08, F03A and F03B).

Table 3. *Filament feedstocks*

Feedstock	MMaster binder	Additives				Powder	
		Backbone	Backbone content (vol.%)*	$S^{\square}$ or P^{x}	$S^{\square}$ or P^{x} (vol.%)	SS 316 L content (vol.%)	Particle size d_{50} (μm)
F01	M1	-	-	-	-	60	6.85
F02	M1	TPE	Y	-	-	60	6.85
F03	M1	TPE	X	$S^{\square}$	5	60	6.85
F04	M1	TPE	X + 5	$S^{\square}$	5	60	6.85
F05	M1	TPE	X + 10	$S^{\square}$	5	60	6.85
F06	M1	TPE	X	P^{x}	5	60	6.85
F07	M1	TPE	W	P^{x}	10	60	6.85
F08	M1	ULD-PE	X	P^{x}	5	60	6.85

* The exact ratio of master binder/backbone in the feedstock will be kept confidential. Y, X and W represent the different amounts of backbone (vol.%).

X = Y – 2.5 vol.%; (½ of S/P content: 5 vol.%).

W = Y – 5 vol.%; (½ of F07 plasticiser (P) content: 10 vol.%).

$S^{\square}$ – Surfactant

P^{x} – Plasticiser

Small pellets of feedstocks were extruded into a filament form. Filament fabrication was performed in a single screw extruder (Brabender GmbH & Co.) with 5 heating zones. The temperature of the zones, from feeder to nozzle (ø 1.75 mm), was set at 160, 165, 170, 175, 180 ˚C. The screw rotation speed was set at 5 rpm. The filament was measured at multiple points to guarantee its dimensional accuracy throughout the filament fabrication process.

Instead of using catalytic debinding, a thermal debinding was selected, since this is an eco-friendly solution. However, it will be necessary to guarantee that no carbonaceous residues are present during sintering. The thermogravimetric analysis highlights that all of the organic constituents of the feedstock fully degrade, during the debinding stage (Fig. 4).

The thermal cycles in this work were selected based on thermogravimetric analysis (TGA). The primary events in the master binder and backbone weight loss curves up to 600 °C (Fig. 4 and Table 4) were the

isothermal plateaus during the debinding stage. The beginning and ending values were evaluated from the first derivative (DTG) of the respective curve. At 495 °C, the carbonaceous residue was close to 0 wt.%.

Concerning the thermal oxidation of the as-received SS 316L powder, TGA showed that it was quite stable up to 600 °C in an N_2 atmosphere. An insignificant increase in the weight of the powder was noticeable above 500 °C. This is not exclusively attributed to the TGA protective atmosphere type (N_2) because other studies show the same behaviour under an Ar + H_2(5%) atmosphere [31, 32].

Table 4. Weight loss and degradation temperatures of the M1, TPE and M1 + TPE

Binder component	Degradation stage	Weight loss [%]	Onset [°C]	End [°C]
M1	1^{st}	41	232	314
	2^{nd}	13	378	437
	3^{rd}	46	437	472
TPE	1^{st}	2	300	327
	2^{nd}	98	408	454
M1 + TPE	1^{st}	35	238	320
	2^{nd}	11	375	398
	3^{rd}	23	427	441
	4^{th}	31	450	475
Plasticiser	1^{st}	100	242	276

A significant difference was not detected in the debinding kinetics of the M1 and TPE as raw materials (Fig. 4) and as feedstocks constituents (Fig. 5) when mixed with 60 vol.% of metallic powder. This is an indication that there are no undesired reactions among the feedstock constituents that could interfere in the debinding cycle.

Table 5 shows a comparison of the theoretical values against the final experimental values (wt.%) of the feedstock filaments at 600 °C in order to illustrate the expected SS 316L weight (%) after binder degradation based on the SS 316L vol.% in the feedstock. The small deviation between theoretical and experimental values can be attributed to the experimental evaluation of the densities and can be assumed that the binder degradation was total.

Table 5. TGA experimental vs theoretical weight reduction of filaments F03, F06 and F08

Feedstock	Metallic powder [wt.%]	
	Experimental	Theoretical*
F03	92.5	92.4
F06	92.5	92.4
F08	92.4	92.4
*Conversion from SS 316L 60 vol.%		

The heating rates for debinding and sintering were 1 °C/min and 10 °C/min up to the maximum temperatures of 600 °C and 1250 °C, respectively. The filaments were debinded and sintered under an H_2 atmosphere at $4x10^{-2}$ MPa.

Results And Discussion

3.1 Feedstock optimisation

3.1.1 Evaluation of the critical powder volume concentration (CPVC)

The evaluation of the CPVC in each feedstock was performed by recording the mixing torque to maximise the metal powder content (vol.%), to promote higher green densities. Nevertheless, MEX feedstocks require overcoming new challenges (rheology and flexibility/stiffness balance) because the filament must be spooled, handled, and extruded through a small-diameter nozzle. Therefore, PIM feedstocks must be modified to be suitable for MEX, and the rheological behaviour of the new feedstock must be studied.

Torque values were recorded for the initial mixture of the master binder and additives F06 (M1 + TPE + P) with 50 vol.% SS 316L powder. The effect of subsequent additions of metallic powder (1 vol.%) on the torque value, shown at every peak from the 10 min. mark was measured after attaining a steady-state regime for each percentage (Fig. 6). Based on this evaluation, the defined ratio of inorganic/organic vol.% among all studied feedstocks was maintained.

Figure 7 shows the torque values for the incremental additions of 1 vol.% of SS 316L powder (50–65 vol.%). Three linear regimes can be observed:

- The first regime includes up to 58 vol.% of SS 316L powder, and the torque variation between each addition is between 1.9 N•m (50 vol.%) and 3.5 N•m (58 vol.%).

- In the second regime, at up to 62 vol.% of SS 316L powder, the mixture rheology changes, which corresponds to a slightly higher slope than the first regime, and the maximum torque is 5.4 N•m.

- The third regime, where the most significant variation occurs (62–65 vol.%), reaches the highest mixing torque value (8.1 N•m). In this range, the mixing torque behaviour clearly becomes more unstable (cf. Fig. 7).

The CPVC should correspond to the interface torque value between the second and third regimes (point of intersection), which in the present study was 62 vol.%. However, a great number of studies performed concerning the optimisation of powder and binder feedstocks show that the torque value should not exceed 5 N.m, to attain the best rheological properties, in order to guarantee optimal processability [29, 33, 34].

Based on the CPVC evaluations (Fig. 6 and 7) and keeping in mind that the feedstock flowability to build the green part, through a 3D printer with a 0.4 mm nozzle, is promoted by the filament (it acts like a piston through the 3D printer pull system) and not by a screw (high pressures), 60 vol.% (torque value of 4.3 N.m) was selected as the metallic load for all studied feedstocks.

3.1.2 Effect of additives in the feedstock

In PIM, the binder generally promotes the best compromise between green integrity and flowability.

However, as previously mentioned, flexibility is one of the major characteristics of MEX filaments. For this reason, the backbone, surfactant and plasticiser content were optimised. To select the best feedstock composition, two different approaches were considered: the addition of TPE + surfactant (S) and the addition of TPE + plasticiser (P).

Figure 8 shows the impact of the additive composition on the final torque value. F01 is a feedstock used in PIM, where there are no concerns about flexibility. In addition to promoting filament flexibility, TPE has a negative impact on the rheological behaviour of the feedstock. To overcome this issue, a surfactant (S) was added. Among the feedstocks in Fig. 8, F03 (blue curve) showed the most promising behaviour (close to 4 N.m).

Although the selected surfactant, stearic acid (SA), clearly reduced the feedstock torque, other mixtures were studied to possibly replace it owing to the difficulty of fully removing it during debinding. Other work reported that SA requires raising the debinding temperature from 600 to 700 °C [31]. Thus, SA was replaced with a plasticiser (P), which also acts as a rheological modifier with the advantage that it promotes filament flexibility.

Figure 9 shows the different torques values for the remaining studied feedstocks (F06–F08). F06 had a final torque (4.6 N•m) that was higher than that of F07 (3.6 N•m) due to its high TPE content. Comparing the feedstocks with the same vol.% of all constituents (F03, F06 and F08), the addition of the surfactant

(F03) had a larger influence on the final torque value than a plasticiser (F06 and F08), as expected. However, the plasticiser boosts filament flexibility, which is a very important requirement.

The feedstock F08, which had the composition as F06 except the TPE was replaced by ULD-PE, had a lower torque value, but it was still higher than the feedstock with SA (F03). Based on torque values of the feedstocks, F06–F08 seem to be suitable for use in MEX.

3.1.3 Influence of metal powder particle size

To evaluate the influence of the SS 316L powder particle size on the rheological behaviour of the feedstock, two mixtures with the same vol.% of SS 316 and additives but different particle sizes were compared: F03A and F03 with d_{50} = 3.76 µm and d_{50} = 6.85 µm, respectively (Fig. 10). The finer particle size led to a higher final mixing torque compared with that of F03. For this reason, powder with d_{50} = 3.76 µm was not selected for the studied feedstocks. This is an expected behaviour as small particles have a high specific surface area of contact, which promotes high interparticle friction [35].

Table 6 summarises the average of ten torque values for each of the different feedstocks.

Table 6. Torque values of different feedstocks

	F01	F02	F03	F04	F05	F06	F07	F08	F03A
Torque [N.m]	2.0	5.5	3.7	4.3	5.3	4.5	3.6	4.2	4.6
Backbone content	-	Y	X	X+5	X+10	X	W	X	X
$S^{\square}$ or P^{X} (vol.%)	-	-	5	5	5	5	10	5	5

3.2 Filaments

3.2.1 Green filament production

In this study, the filament was not spooled by an automatic system. To avoid filament diameter deviations due to gravity action, a constant height between the extruder nozzle and the table was preserved for all formulations.

Standard filament (powder and binder – F01) was too brittle to spool. The other feedstocks (powder, binder and additives) could be spooled (F03, F04, F05 and F08), but with a higher curvature than those of F07 and F06 (Fig. 11). It must be emphasised that the best filaments were those resulting from feedstocks with plasticizer and torque close to 5.0 N•m.

3.2.2 Characterization

3.2.2.1 Homogeneity

SEM observations of the filament cross-section shown that filament feedstocks without TPE (F01 and F08) appeared to be more homogeneous than the others (F03 and F06, Fig. 12), but their flexibility was poor. F03 and F06 (= M1 + TPE + S/P vol.%) were quite similar regarding the homogeneity of the distribution of metallic powder. A large powder particle distance in the feedstocks improves flexibility but decreases density. Thus, considering these two features (filament flexibly and interparticle distance), a homogenous powder distribution is crucial and a suitable balance between these features is required for the success of MEX.

Micro-CT analysis can be an effective solution for assessing filament homogeneity without fracture, which can modify the defect distribution on the observed volumes. Micro-CT was performed in a representative cross-section of filament F06 in the green and sintered states (Fig. 13a and b, respectively). It can be noted that the green filament (extruded feedstock in filament form, not subject to any subsequent processing step) presents a high density and consistent diameter throughout its section, reiterating the mechanical behaviour results (cf. 3.2.2.3). The observed residual pores seem to follow the extrusion direction (Fig. 13a, X-Z and Z-Y section), suggesting that the defects may occur in the extrusion process, resulting in elongated pore geometry. Nevertheless, the sintered filament shows that a sintered part with consistent density is still achievable, indicating that resulting porosity in final parts may be connected to printing parameters.

3.2.2.2 Structure

The X-ray diffractograms (Fig. 14) show the evolution from SS 316L powder to the green and sintered filament. As referred, the austenitic powder, owing to its preparation technique, besides austenite (ICDD 33-0397), presents a ferrite/martensite phase (ICDD 87-0722 - Fig. 3). This one increases, as expected, due to the deformation of powders during its extrusion (Fig. 14). However, after sintering, the X-ray diffractogram shows only constituted by the austenitic phase, avoiding a post heat treatment, required in other additive processes.

3.2.2.3 Mechanical behaviour

The deflection at rupture (%) and flexural modulus of elasticity (E_{flex}) was measured by three-point bending tests (Fig. 15). Each value in the figure is the average of five tests. These results, together with the previous torque rheometry study, allowed for selecting the most promising filament feedstocks regarding green processability.

The filament from feedstock F01, without additives, was the most brittle (13%). With the incremental addition of TPE to feedstocks F03–F05, the maximum deflection of the filaments increased. However, as previously discussed, F05 was not produced in filament form owing to its high torque value, which was

promoted by the high amount of TPE (vol.%). Comparing filaments F03 and F06 (equal vol.% of organic constituents), the replacement of the surfactant with a plasticiser improved the flexibility. A reduction in deflection from F06 (91%) to F07 (71%) was noticeable. F07 had the highest additive content and, consequently, less TPE in the feedstock. F08 had ULD-PE instead of TPE. The reduction in the F08 filament flexibility (44%) is more obvious compared to that of F06, which had the same additive, a plasticiser. In fact, filament from feedstock F08 was not used to produce the green parts because it was brittle, despite its promising mixing torque (4.2 N•m).

The E_{flex} results of F07 and F08 were not expected, taking into account the relationship between the maximum deflection at break and the E_{flex} of the remaining filaments. This can be attributed to several factors, including porosity and the non-homogeneous feedstock mixture. Similar behaviour was also reported by another study [20].

Conclusions

High-quality filaments for metallic MEX can be attained by optimization of different manufacturing steps: feedstocks production (metallic powder, binder and additives), evaluation of extrudability (torque <4.0-4.5 N•m, supported by other rheological studies), debinding and sintering. In the filament feedstocks, the main challenges are to reach the highest metallic powder content with good extrudability and a suitable ratio between stiffness and flexibility. Some filaments, without surfactant/plasticizer or with different additive contents, are unsuitable due to the difficulty to be extruded, owing to their high mixing torque.

From the extruded feedstocks, the selected case study shows that, for the filament constituted by SS 316L + M1 + TPE + P, the best green mechanical characteristics are attained due to the excellent homogenization of the mixing, demonstrated by micro-CT. Moreover, the best filament, after debinding and sintering, continues to show excellent performance, concerning defects (porosity) and consequently, the best flexural modulus and deflection at break, assuring an excellent MEX processability. In the case of austenitic steel powders, the austenite phase is the only phase present, avoiding other costly post heat treatments.

In conclusion, this study promotes a supported methodology for producing filaments for MEX from metallic powders.

Declarations

Funding This work was supported by the European Regional Development Fund (ERDF) under the Portuguese program—Programa Operacional Factores de Competitividade (COMPETE) [grant agreement No. POCI-01-0247-FEDER-024533]; and this research is sponsored by FEDER funds through the program COMPETE – Programa Operacional Factores de Competitividade – and by national funds through FCT – Fundação para a Ciência e a Tecnologia -, under the project UIDB/00285/2020.

Conflicts of interest The authors declare that they have no conflict of interest.

Availability of data and material Data will be available upon request.

References

1. Alcácer V, Cruz-Machado V (2019) Scanning the Industry 4.0: A Literature Review on Technologies for Manufacturing Systems. Engineering Science and Technology, an International Journal 22:899. https://doi.org/10.1016/j.jestch.2019.01.006
2. Dilberoglu UM, Gharehpapagh B, Yaman U, Dolen M (2017) The Role of Additive Manufacturing in the Era of Industry 4.0. Procedia Manufacturing 11:545. https://doi.org/10.1016/j.promfg.2017.07.148
3. Additive Manufacturing Wohlers Report 2018 Shows Rise in Metal Additive Manufacturing. https://www.additivemanufacturing.media/news/wohlers-report-2018-shows-rise-in-metal-additive-manufacturing. Accessed 22 Feb 2019
4. Clemens Lieberwirth, Arne Harder, Hermann Seitz (2017) Extrusion Based Additive Manufacturing of Metal Parts. JMEA 7:. https://doi.org/10.17265/2159-5275/2017.02.004
5. Gong H, Crater C, Ordonez A, et al (2018) Material Properties and Shrinkage of 3D Printing Parts using Ultrafuse Stainless Steel 316LX Filament. MATEC Web Conf 249:01001. https://doi.org/10.1051/matecconf/201824901001
6. Thompson Y, Gonzalez-Gutierrez J, Kukla C, Felfer P (2019) Fused filament fabrication, debinding and sintering as a low cost additive manufacturing method of 316L stainless steel. Additive Manufacturing 30:100861. https://doi.org/10.1016/j.addma.2019.100861
7. (2020) Making Additive Manufacturing Sustainable: Ask the Right Question. tct MAG 28:24–25
8. Lingqin X, Guang C, Luyu Z, Pan L (2020) Explore the feasibility of fabricating pure copper parts with low-laser energy by selective laser melting. Mater Res Express 7:106509. https://doi.org/10.1088/2053-1591/abbd08
9. Ikeshoji T-T, Nakamura K, Yonehara M, et al (2018) Selective Laser Melting of Pure Copper. JOM 70:396–400. https://doi.org/10.1007/s11837-017-2695-x
10. Godec D, Cano S, Holzer C, Gonzalez-Gutierrez J (2020) Optimization of the 3D Printing Parameters for Tensile Properties of Specimens Produced by Fused Filament Fabrication of 17-4PH Stainless Steel. Materials 13:774. https://doi.org/10.3390/ma13030774
11. Thompson Y, Gonzalez-Gutierrez J, Kukla C, Felfer P (2019) Fused filament fabrication, debinding and sintering as a low cost additive manufacturing method of 316L stainless steel. Additive Manufacturing 30:100861. https://doi.org/10.1016/j.addma.2019.100861
12. ISO/ASTM Additive manufacturing - General principles - Terminology (ISO/ASTM DIS 52900:2018)
13. Ziaee M, Crane NB (2019) Binder jetting: A review of process, materials, and methods. Additive Manufacturing 28:781–801. https://doi.org/10.1016/j.addma.2019.05.031
14. Bai Y, Williams CB (2018) Binder jetting additive manufacturing with a particle-free metal ink as a binder precursor. Materials and Design 11

15. Bai Y, Wagner G, Williams CB (2017) Effect of Particle Size Distribution on Powder Packing and Sintering in Binder Jetting Additive Manufacturing of Metals. Journal of Manufacturing Science and Engineering 139:081019. https://doi.org/10.1115/1.4036640
16. Singh P, Balla VK, Tofangchi A, et al (2020) Printability studies of Ti-6Al-4V by metal fused filament fabrication (MF3). International Journal of Refractory Metals and Hard Materials 91:105249. https://doi.org/10.1016/j.ijrmhm.2020.105249
17. Danforth SC, Agarwala M, Bandyopadghyay A, et al (1998) Solid freeform fabrication methods. 17
18. Gonzalez-Gutierrez J, Cano S, Schuschnigg S, et al (2018) Additive Manufacturing of Metallic and Ceramic Components by the Material Extrusion of Highly-Filled Polymers: A Review and Future Perspectives. Materials 11:840. https://doi.org/10.3390/ma11050840
19. M K Agarwala, Weeren, R. van, Bandyopadhyay, A., et al (1996) Fused Deposition of Ceramics and Metals: An Overview. In: International Solid Freeform Fabrication Symposium. Texas, USA, p 8
20. Kukla C, Duretek I, Schuschnigg S, Gonzalez-Gutierrez J (2016) Properties for PIM Feedstocks Used in Fused Filament Fabrication. In: Proceedings of the World PM2016 Congress & Exhibition. Hamburg, Germany, 9–13 October 2016, p 5
21. Gonzalez-Gutierrez J, Godec D, Kukla C, et al (2017) Shaping, Debinding and Sintering of Steel Components via Fused Filament Fabrication. Croatian Association of Production Engineering, Zagreb, pp 99–104
22. Burkhardt C, Freigassner P, Weber O, et al (2016) Fused Filament Fabrication (FFF) of 316L Green Parts for the MIM process. In: Proceedings of the World PM2016 Congress & Exhibition. EPMA, Hamburg, Germany, 9–13 October 2016, pp 1–7
23. Andersen O, Riecker S, Studnitzky T, et al (2018) Manufacturing and Properties of Metal Parts made by Fused Filament Fabrication. In: Euro PM2018 Proceedings. EPMA, Bilbao, Spain, 14 – 18 October 2018, pp 1–6
24. Kurose T, Abe Y, Santos MVA, et al (2020) Influence of the Layer Directions on the Properties of 316L Stainless Steel Parts Fabricated through Fused Deposition of Metals. Materials 13:2493. https://doi.org/10.3390/ma13112493
25. Gloeckle C, Konkol T, Jacobs O, et al (2020) Processing of Highly Filled Polymer–Metal Feedstocks for Fused Filament Fabrication and the Production of Metallic Implants. Materials 13:4413. https://doi.org/10.3390/ma13194413
26. Nestle, Nikolaus, Hermant, Marie-Claire, Schmidt, Kris (2016) Mixture for use in a fused filament fabrication process. 40
27. Randall M. German, Animesh Bose (1997) Injection Molding of Metals and Ceramics. Metal Powder Industry, Princeton, N.J.
28. Vieira MT, Martins AG, Barreiros FM, et al (2008) Surface modification of stainless steel powders for microfabrication. Journal of Materials Processing Technology 201:651. https://doi.org/10.1016/j.jmatprotec.2007.11.162

29. T.J. Ferreira, M.T. Vieira (2017) Optimization of MWCNT – Metal Matrix Composites feedstocks. Ciência & Tecnologia dos Materiais 29:87–91. https://doi.org/10.1016/j.ctmat.2016.07.010
30. Carreira P, Cerejo F, Alves N, Vieira MT (2020) In Search of the Optimal Conditions to Process Shape Memory Alloys (NiTi) Using Fused Filament Fabrication (FFF). Materials 13:4718
31. Telma Joana Jesus Ferreira (2018) Microinjection Moulding of Austenitic Stainless Steel Reinforced with Carbon Nanotubes. PhD Thesis, University of Coimbra
32. F. Cerejo, A. M. Raimundo, M.T. Vieira, F. M. Barreiros (2019) Fused Deposition of WC+Co powder. EPMA, Maastricht Exhibition & Congress Centre, Maastricht, The Netherlands
33. T.J. Ferreira, M.T. Vieira (2014) Behaviour of feedstocks reinforced with nanotubes for micromanufacturing. In: Euro PM 2014 Congr. Exhib. Proc. EPMA, The Messezentrum Salzburg, Austria
34. Dimitri C, Mohamed S, Thierry B, Jean-Claude G (2017) Influence of particle-size distribution and temperature on the rheological properties of highly concentrated Inconel feedstock alloy 718. Powder Technology 322:273–289. https://doi.org/10.1016/j.powtec.2017.08.049
35. Ibrahim, Mohd Halim Irwan, Norhamidi Muhamad, Abu Bakar Sulong (2011) Rheological Characterization of Water Atomised Stainless Steel SS316L for Micro MIM. Advanced Materials Research 264–265:129–134

Figures

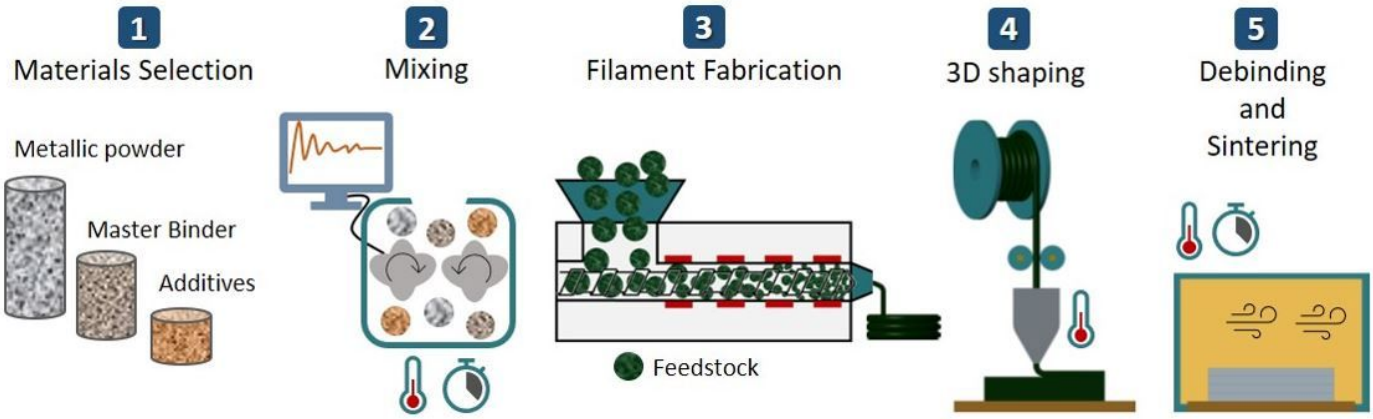

Figure 1

MEX manufacturing route through the shaping, debinding and sintering (SDS) process

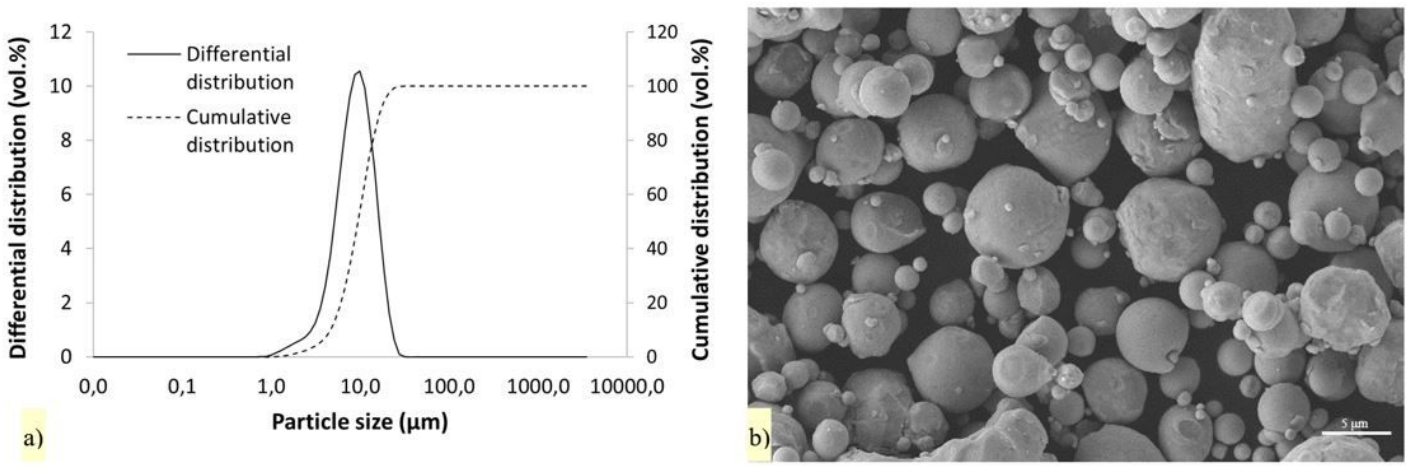

Figure 2

a) Particle size distribution (Malvern Mastersizer 2000) and b) powder shape (SEM analysis, SE) of the SS 316L powder

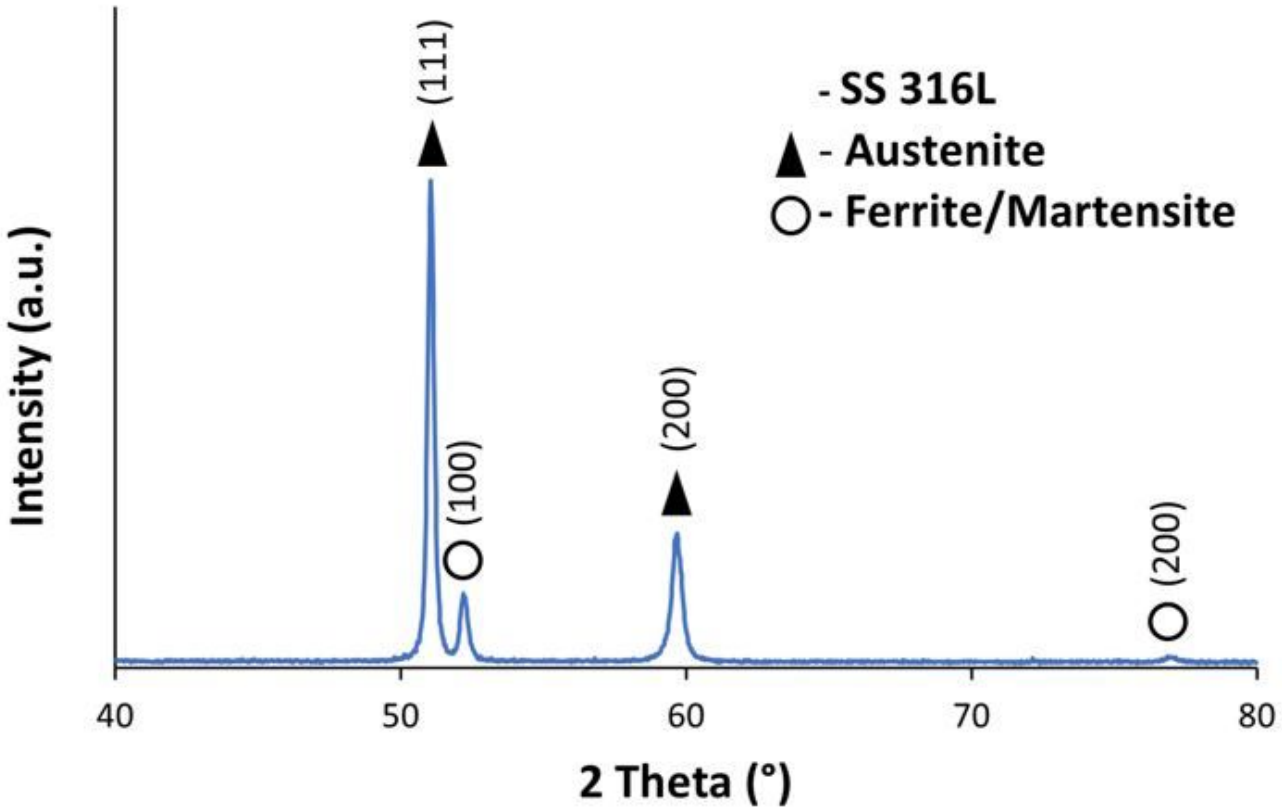

Figure 3

SS 316L XRD diffractogram; λ Co = 0.1789 nm (Philips X'Pert)

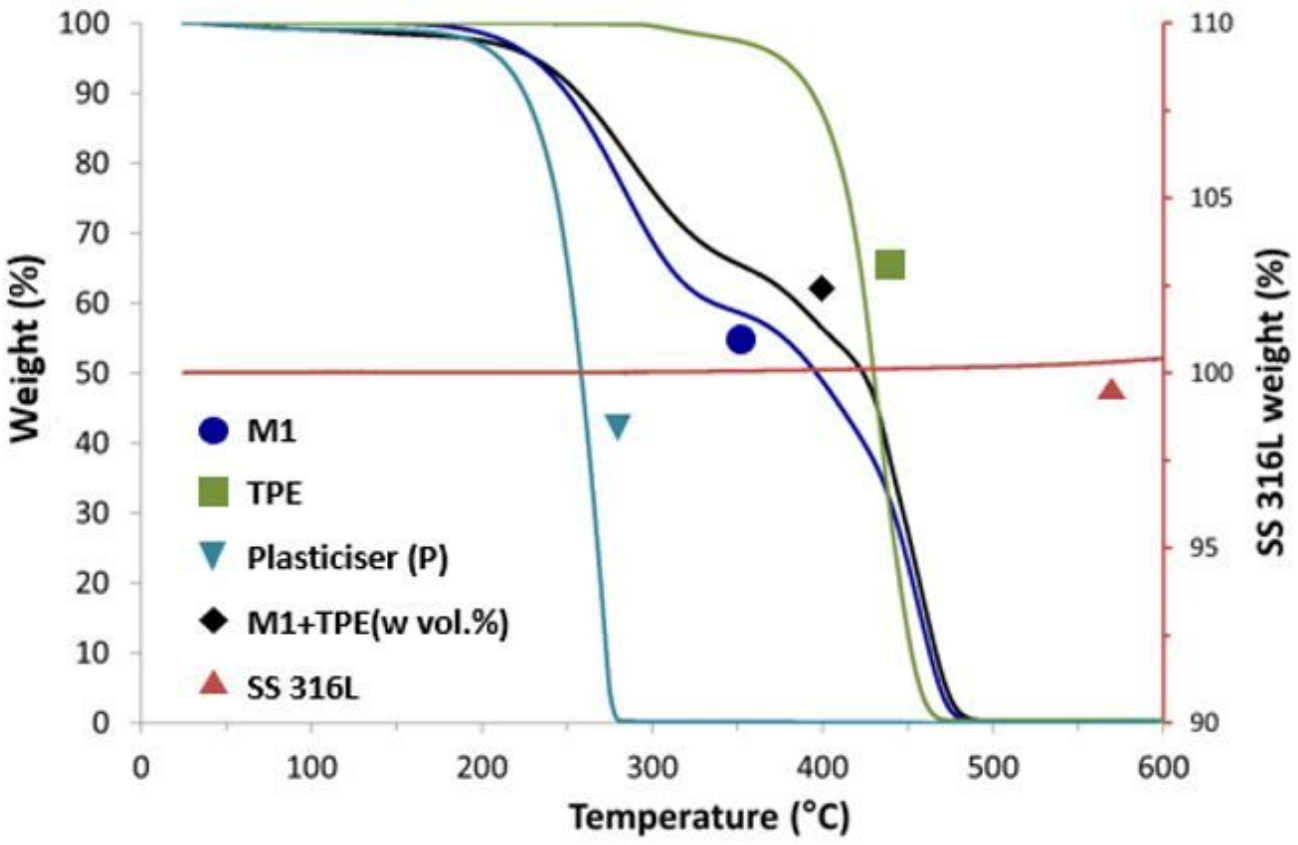

Figure 4

TGA curves of the SS 316L, M1, TPE and M1 + TPE under an N2 atmosphere

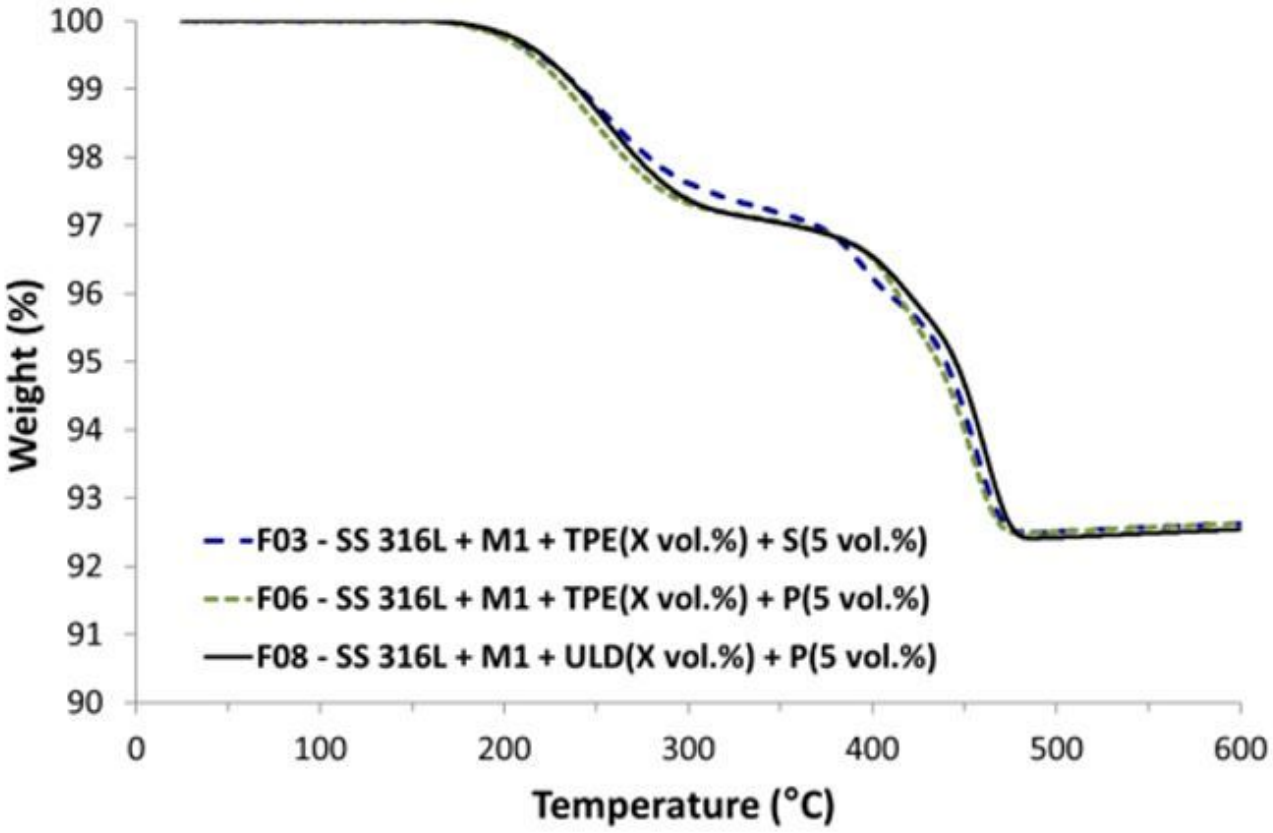

Figure 5

TGA curves of the filaments F03, F06 and F08 with 60 vol.% of SS 316L powder under an N2 atmosphere

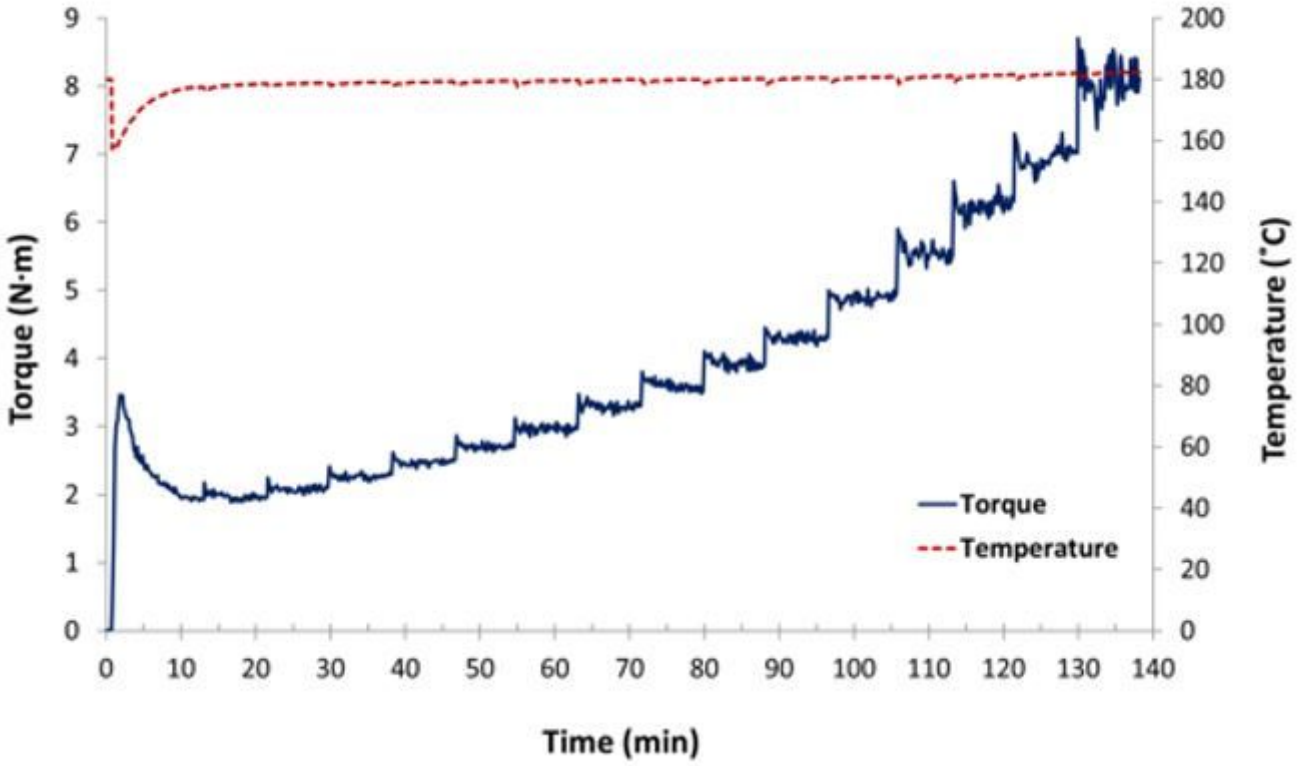

Figure 6

Torque as a function of time of the F06 feedstock at 180 °C with the incremental addition of 1 vol.% of SS 316L

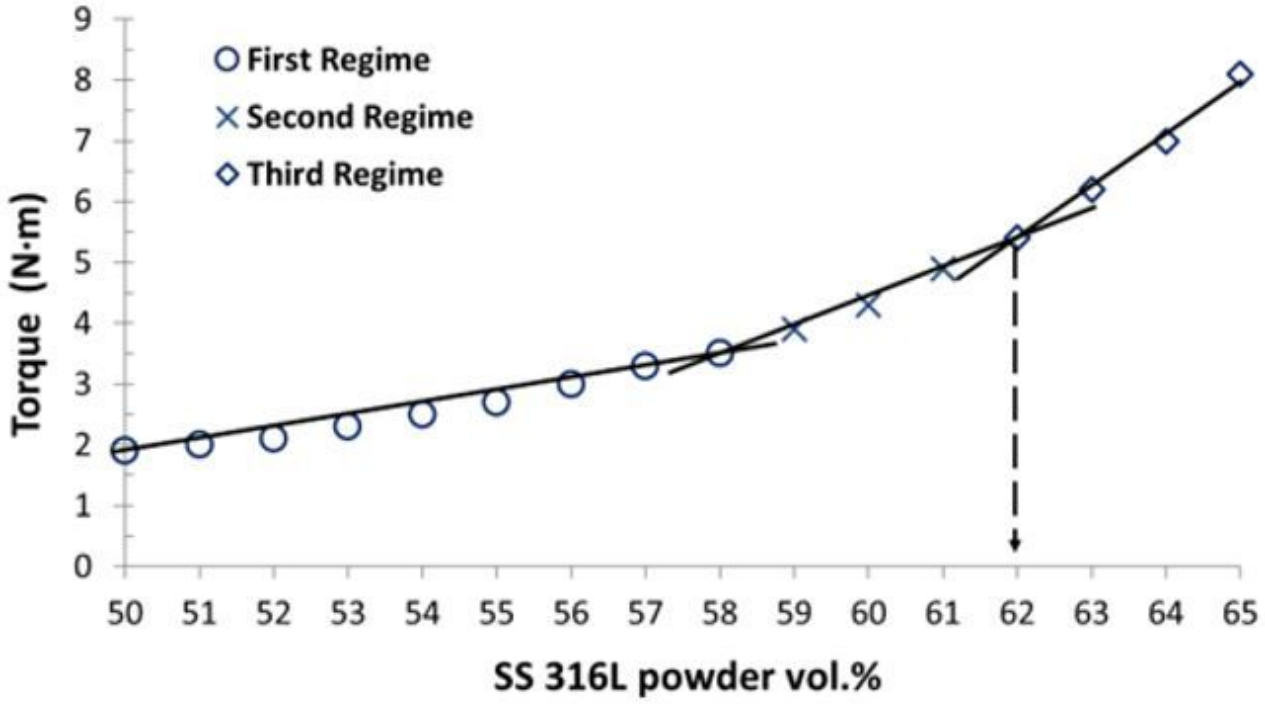

Figure 7

Three different regimes of torque as a function of powder volume concentration (feedstock F06)

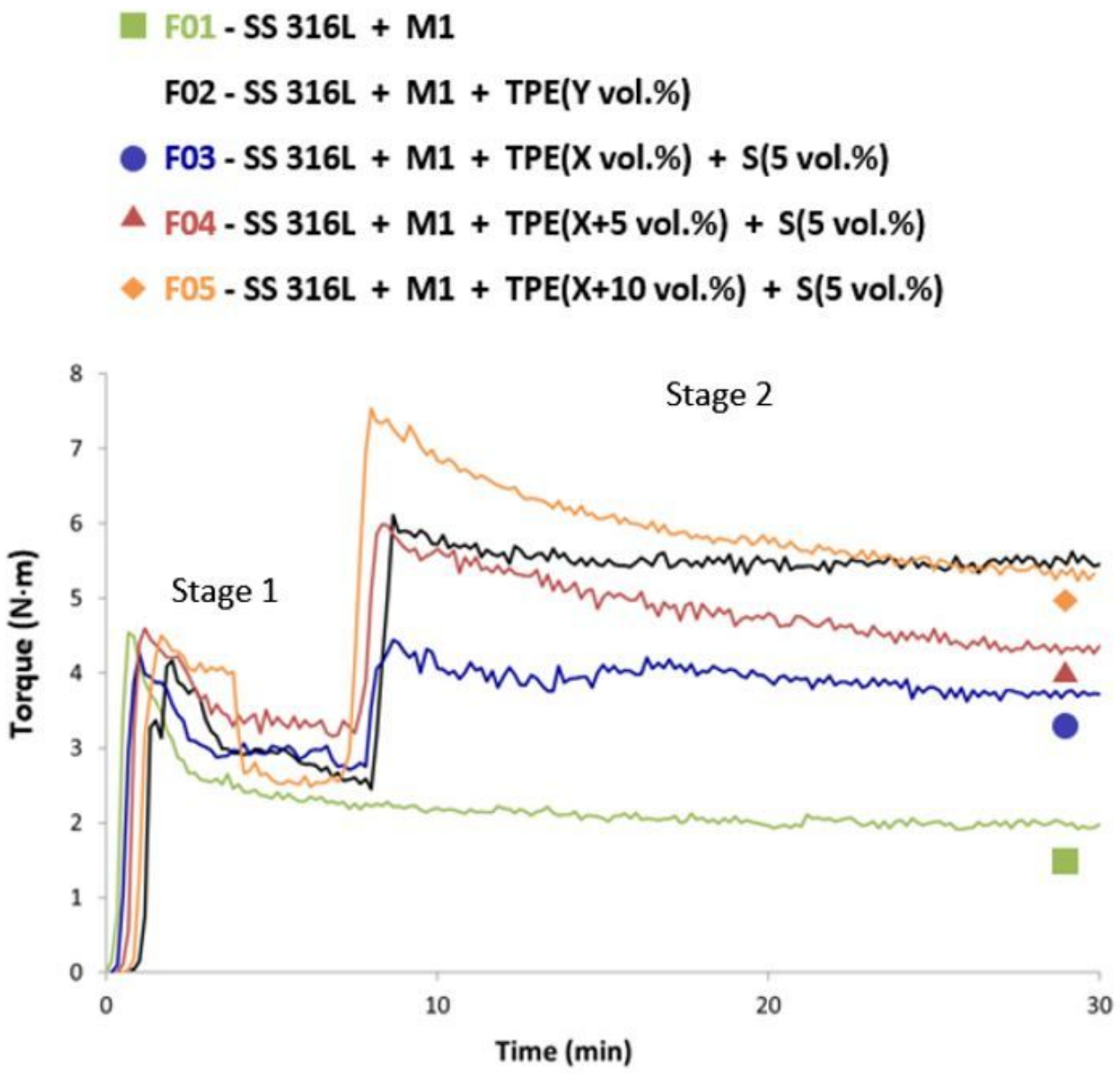

Figure 8

Mixing torques (F01-F05) as a function of time (Y < X vol.%.); Stage 1 - only binder addition; Stage 2 – feedstock with additive addition. F01 is the standard feedstock without additives.

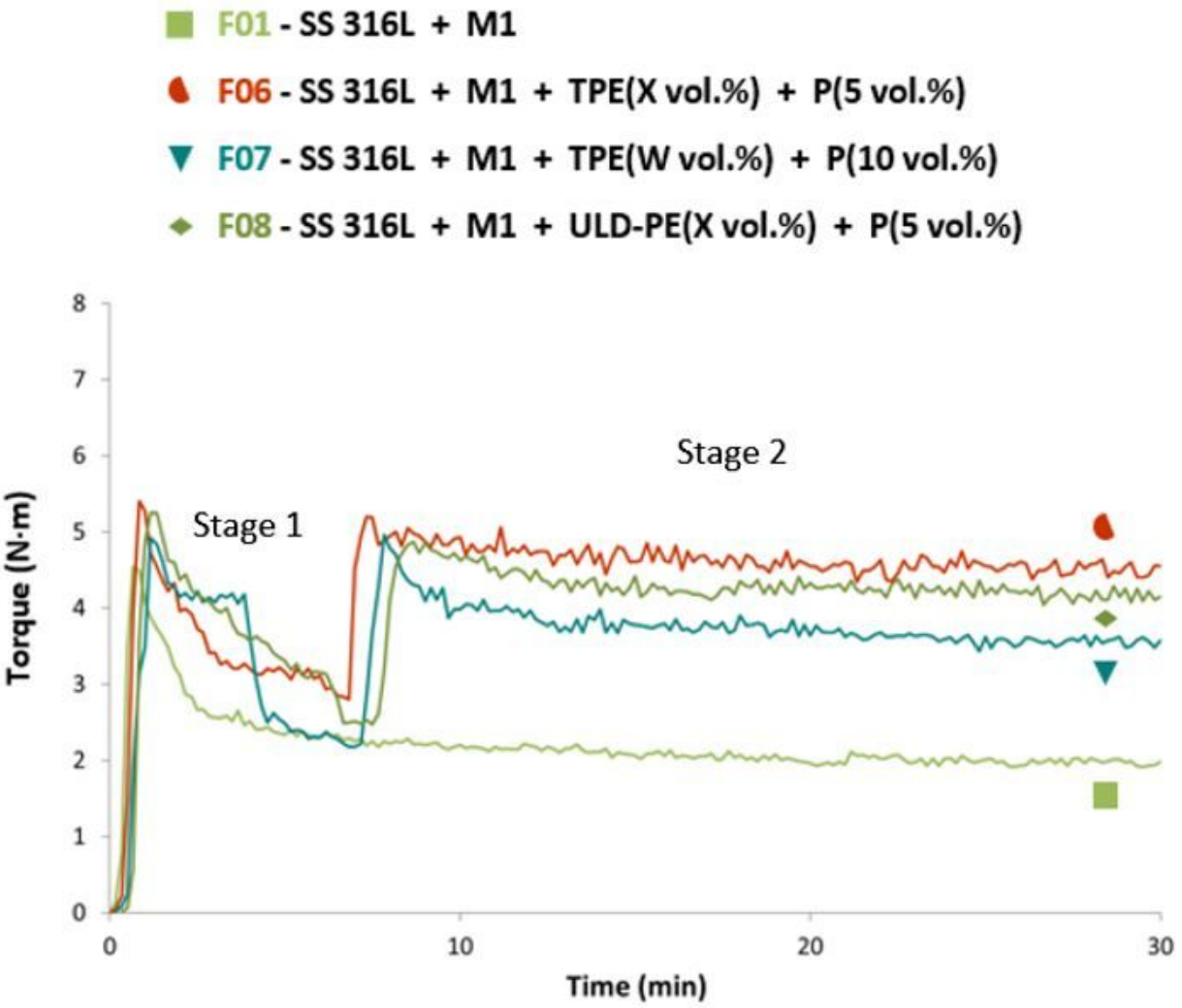

Figure 9

F01 and F06–F08 mixing torques as a function of time (W < X vol.%); Stage 1 - only binder addition; Stage 2 – feedstock with additive addition. F01 is the standard feedstock without additives

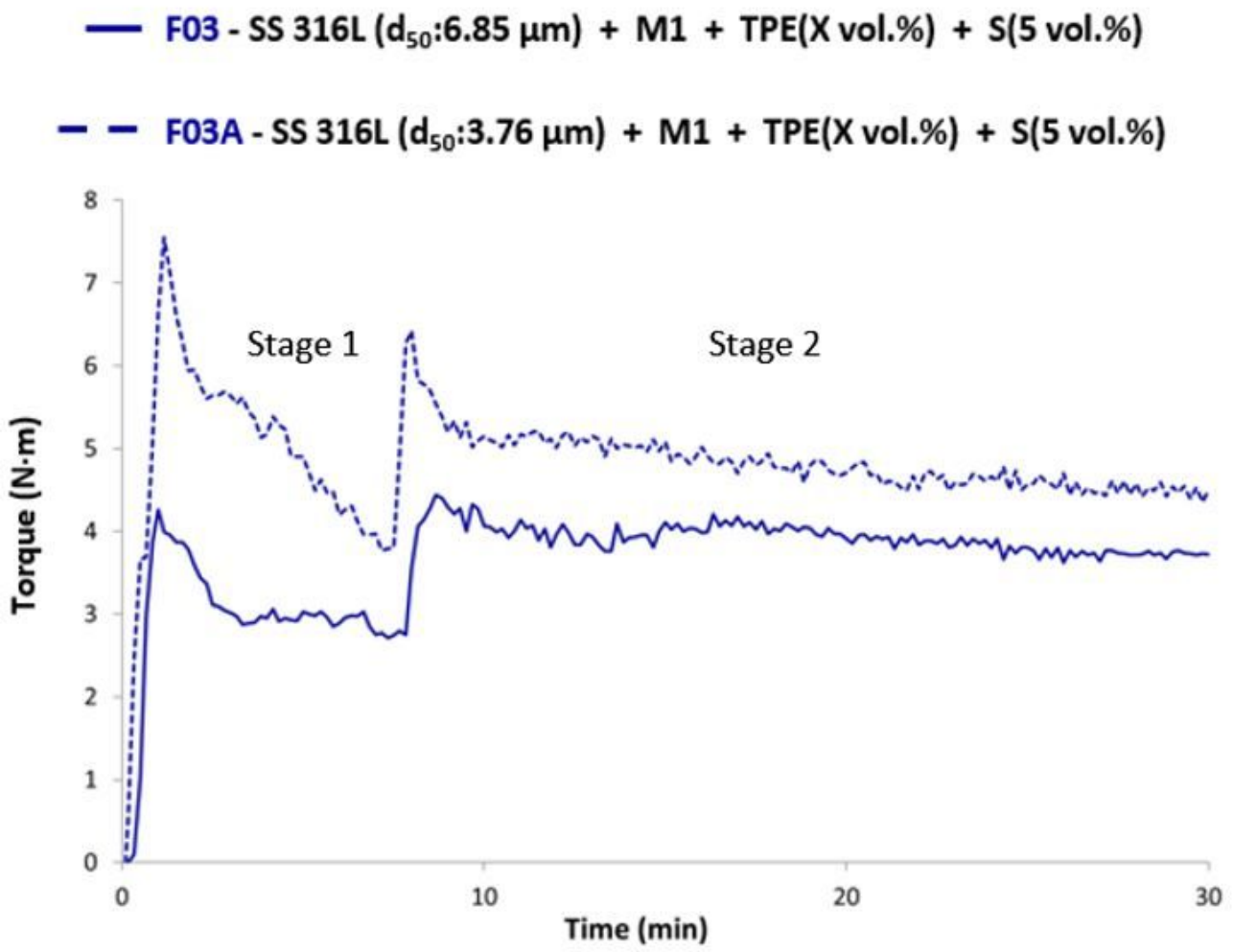

Figure 10

Torque of the F03A and F03 mixtures as a function of time; Stage 1 - only binder addition; Stage 2 – feedstock with additive addition

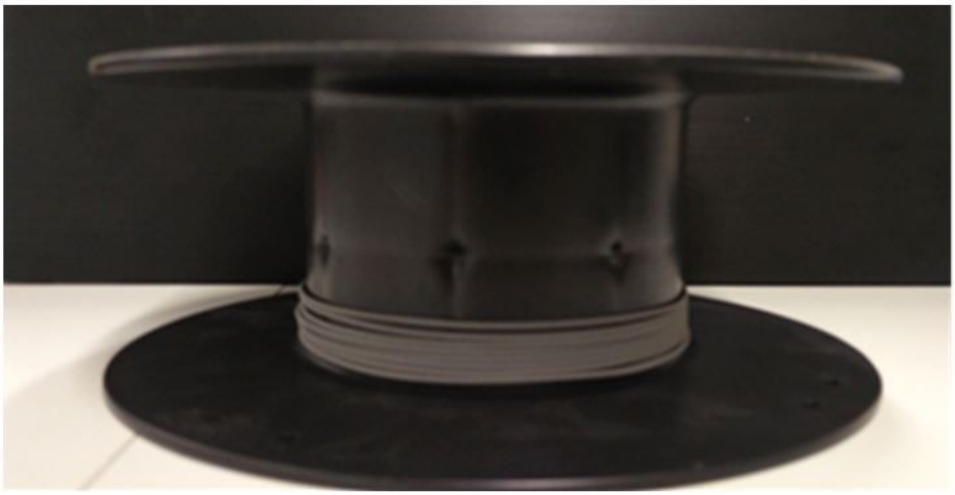

Figure 11

Spooled filament from feedstock F06

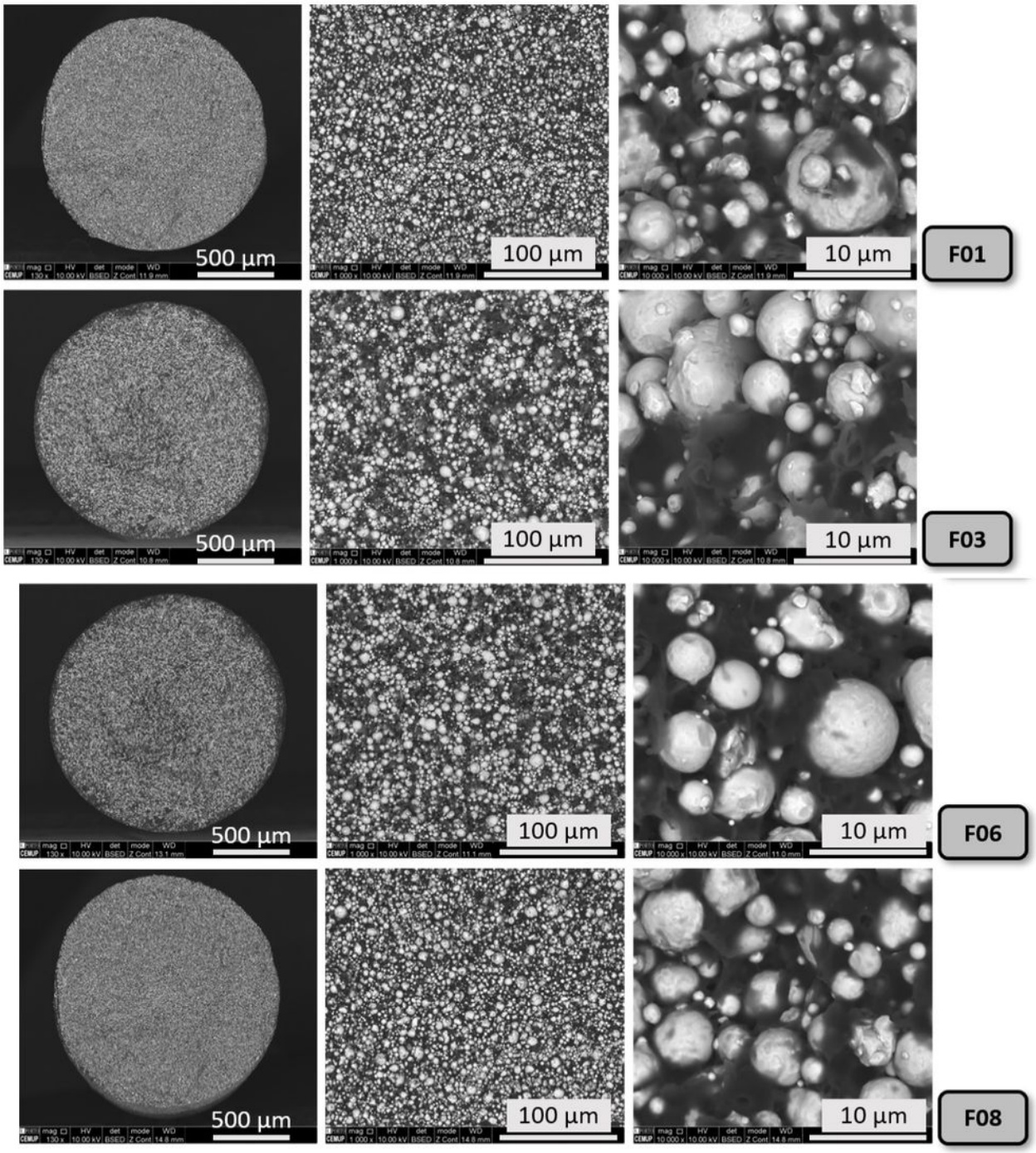

Figure 12

Cross-section fracture surfaces of filaments F01, F03, F06 and F08

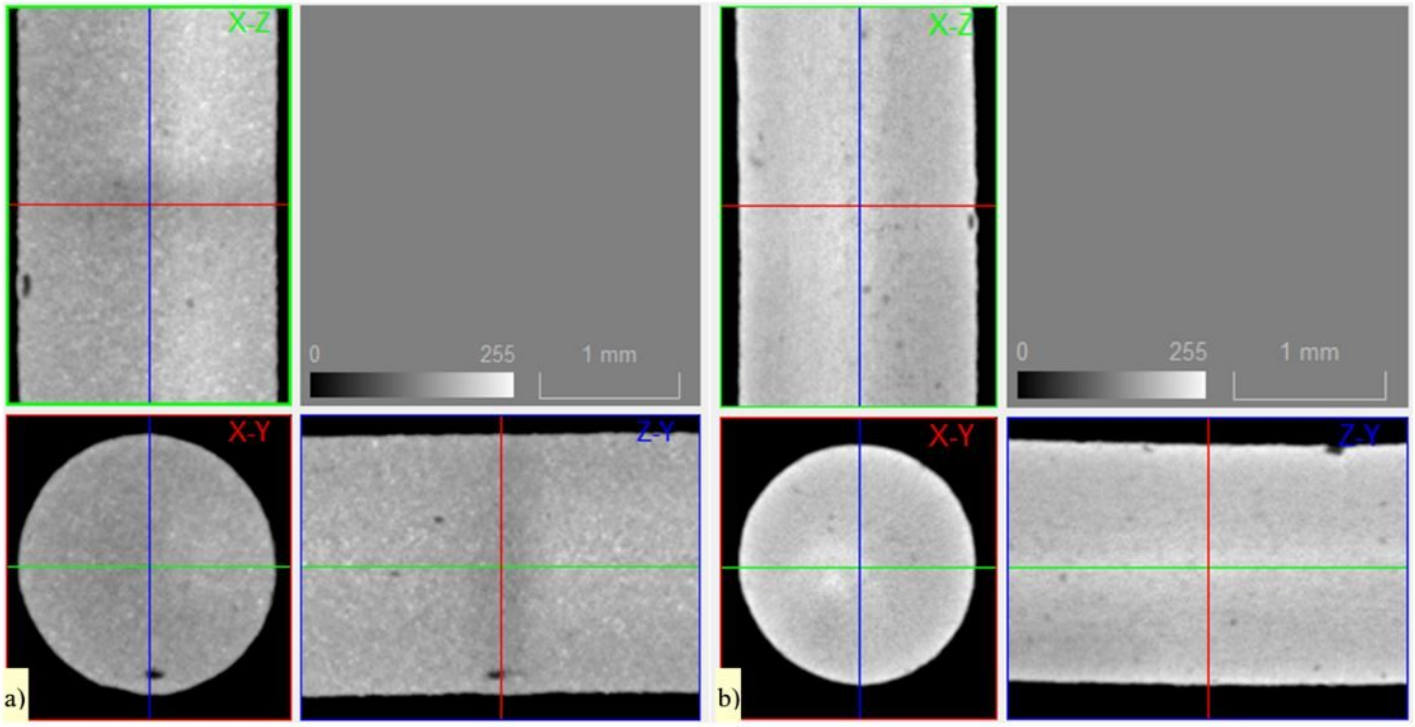

Figure 13

Micro-CT of the a) green filament F06 b) sintered filament F06 – green filament with the highest homogeneity

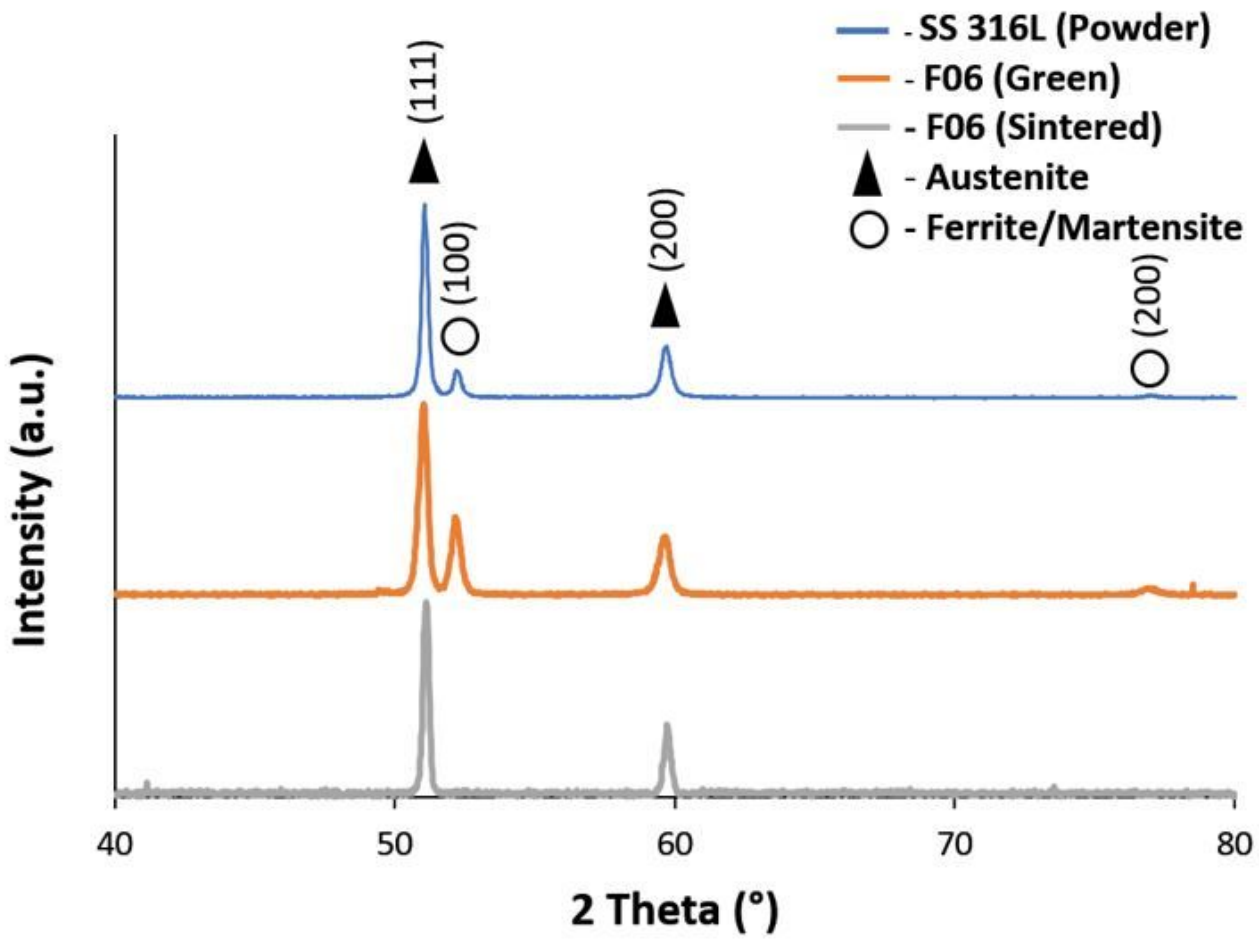

Figure 14

X-ray diffraction of the sintered filament F06

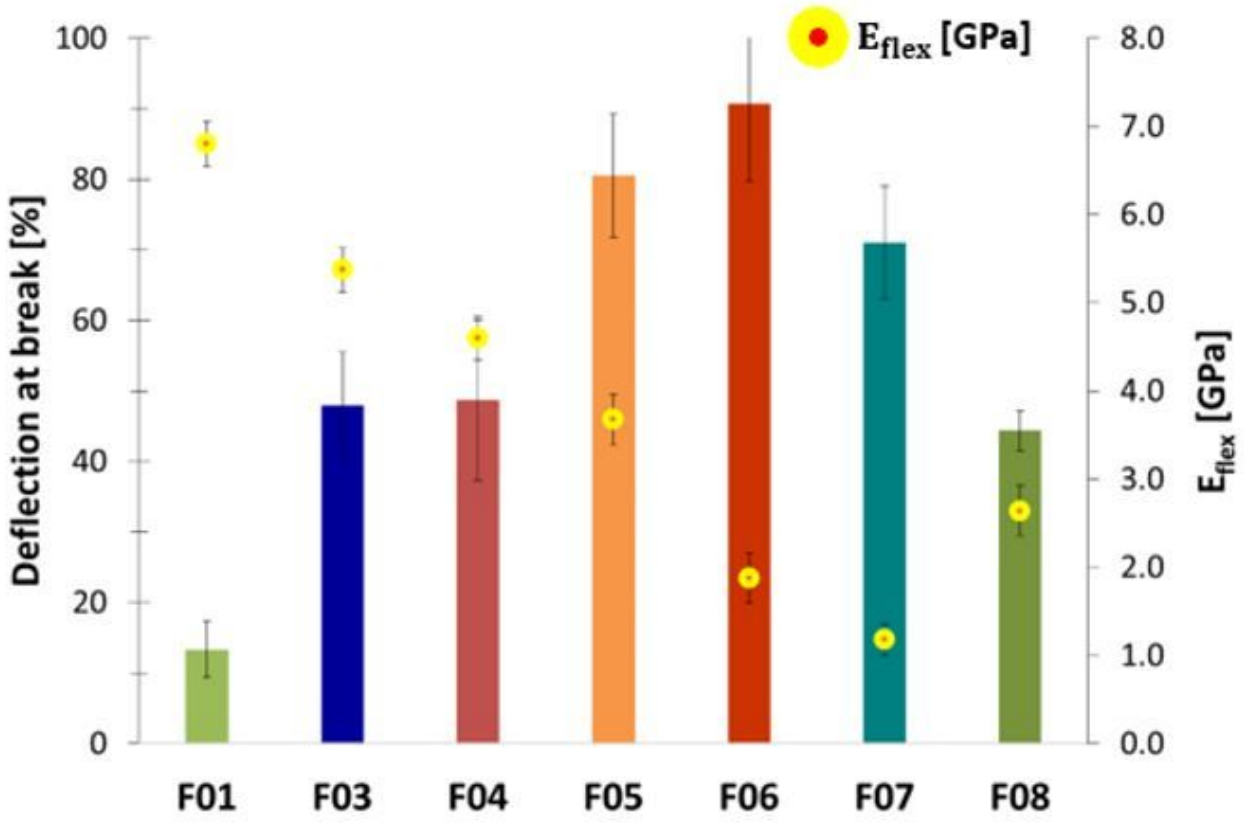

Figure 15

Deflection at break (%) and Eflex of filaments F01 and F03–F08